ELSEVIER

Journal of Chromatography A, 772 (1997) 49–62

JOURNAL OF CHROMATOGRAPHY A

Transient modelling of capillary electrophoresis Isotachophoresis

Johannes H.P.A. Martens[a,*], Jetse C. Reijenga[a], Johannes H.M. ten Thije Boonkkamp[b], Robert M.M. Mattheij[b], Frans M. Everaerts[a]

[a]*Department of Chemical Engineering, Eindhoven University of Technology, P.O. Box 513, NL-5600 MB Eindhoven, The Netherlands*
[b]*Department of Mathematics and Computing Science, Eindhoven University of Technology, P.O.Box 513, NL-5600 MB Eindhoven, The Netherlands*

Abstract

Different algorithms for transient modelling of capillary electrophoresis have been described in several papers. Programs based on such algorithms were applied to various modes of CE. Surprisingly, simulations of capillary isotachophoresis (cITP) at realistic current densities (>1 kA/m^2) were not reported. Using these programs for practical cITP conditions resulted in either severe oscillations, mass-balance violation or unexpected program termination. This paper addresses several numerical paths available for modelling one-dimensional capillary electrophoretic behaviour. Tests for determining the validity of the presented solutions with respect to cITP were mass balance checks, zone boundary thickness and the Kohlrausch regulating function. Six different numerical schemes fulfilled these requirements, yet only few could be used for simulating practical current density situations without causing the aforementioned problems. Attention was paid to space discretization (central difference and quadratic upwind) and time integration (implicit, explicit). A single computer program comprising these strategies was developed. Special features for studying transient state phenomena were visualization of concentrations, velocities, Peclet and Courant numbers, electric field strength, conductivity, pH, buffering capacity and charge excess. All parameters could be displayed in both the space domain (profile) as well as in the time domain (electropherogram).

Keywords: Isotachophoresis; Computer simulation; Computer modelling

1. Introduction

Computer simulations of electrophoretic separations have been described in several textbooks [1,2] and a number of papers [3–10] published in recent years. Although the basic differential equations governing such separations are well defined, it appears from the literature that different numerical approaches for solving the equations can be chosen. In the textbook by Mosher et al. [2] and related papers, a conventional central difference scheme was used and no attention was paid to alternative numerical methods. It took until a series of publications by Ermakov et al. [5,8–10] before this topic was addressed. There it was shown that addition of several artificial dispersion terms to the convection–diffusion equation greatly improved the simulation results, diminishing numerical oscillations and diffusion. The reason for the occurrence of oscillations is that, next to the numerical method chosen, numerical parameters within that method, such as temporal and spatial grid size, are involved. In order to speed-up

*Corresponding author.

PII S0021-9673(97)00121-0

calculations, these should be as large as possible without leading to oscillations and negative concentrations. The optimal values for these parameters depend largely on the electrophoretic conditions chosen (mainly ionic strength and current density). Also, during stacking with resulting electric field strength gradients, the optimum grid sizes may differ from the ones found in later stages of the separation. In Dose's approach [4], such grid size optimization was included, although for strong ions only. Schwer et al. [6] have subsequently extended Dose's approach to include weak ions as well, although simulations were limited to pH ranges where either H^+ or OH^- predominate.

Summarizing, there are a number of numerical approaches available, which are limited in both applicability of practical conditions and calculation speed. By using several alternate numerical approaches these limitations were dealt with. Another (minor) point that the existing programs have in common is the lack of a practical user-interface, which makes it impossible for other people to use the software as if it were a word processor. As will be described, this requirement was met.

2. Materials and methods

Two versions of the program, targeted at different operating systems, were created. The MS-DOS v6.22 (Microsoft, Redmond, WA, USA) version was developed using PowerBasic v3.2 (PowerBasic, Carmel, CA, USA). A single-line single-key sub-menu structure, as used in previously reported simulation software for GC, steady-state CZE (HPCESIM) and MECC [11], was implemented. The Win32 (Windows 95/Windows NT; Microsoft) targeted version was developed using Visual C++ v4.0 (Microsoft). Both programs used an existing database of mobility and pK data of more than 300 components, developed for the already mentioned simulators. These data were taken mainly from the tables compiled by Hirokawa and co-workers [12–14].

Program development and simulations were carried out on 120/133 MHz Pentium computers with 16–32 MB RAM internal memory.

3. Capillary electrophoresis model

The simplest model for electrophoretic processes is a one-dimensional convection–diffusion equation.

$$\frac{\partial C_i(z,t)}{\partial t} = D_i \frac{\partial^2 C_i(z,t)}{\partial z^2} - \frac{\partial (v_i(z,t) C_i(z,t))}{\partial z} \qquad (1)$$

This partial differential equation holds for every component i, at space coordinate z and time t. The concentration C_i needs to be calculated from the diffusion coefficient D_i and the net component velocity v_i. The convection term introduces interrelation of the differential equations for all components through the pH dependent mobilities and the electric field strength

$$v_i(z,t) = (m_{\mathrm{eof}} + m_i(z,t)) \cdot E(z,t) \qquad (2)$$

where m_{eof} is the electroosmotic mobility, m_i is effective mobility of component i and E the local electric field strength.

Since $E(z,t)$ depends on all local concentrations $C_i(z,t)$, mobilities $m_i(z,t)$ and the local pH, Eq. (1) is actually a set of interrelated equations, that need solving at the same time. The mobilities in turn depend on the local pH.

Knowing the acidic constant $K_{i,j}$ for each component's subspecies, and the local hydrogen concentration C_{H} (from the pH), the degrees of dissociation $\alpha_{i,j}$ for subspecies j of component i can be calculated by

$$\alpha_{i,j}(z,t) = \frac{\prod_{p=1}^{j} \frac{K_{i,p}}{C_{\mathrm{H}}(z,t)}}{1 + \sum_{q=1}^{j} \prod_{r=1}^{q} \frac{K_{i,r}}{C_{\mathrm{H}}(z,t)}} \quad (j = 1 \ldots n_i) \qquad (3)$$

in which i ranges over the number of components and j ranges over the number of charged subspecies n_i of component i and

$$\alpha_{i,0}(z,t) = 1 - \sum_{j=1}^{n_i} \alpha_{i,j}(z,t) = \frac{1}{1 + \sum_{q=1}^{j} \prod_{r=1}^{q} \frac{K_{i,r}}{C_{\mathrm{H}}(z,t)}} \qquad (4)$$

From Eqs. (3) and (4) the local (signed) effective mobility m_i can be calculated if the absolute mo-

bilities of the subspecies at infinite dilution, $m^0_{i,j}$, are known

$$m_i(z,t) = \sum_{j=1}^{n_i} \alpha_{i,j}(z,t) m^0_{i,j} \tag{5}$$

Corrections of quantities (e.g., mobilities, acidic constants) for different ionic strengths and temperatures are not introduced into the set of equations, but could be a valuable extension of the current model.

Once the concentrations and mobilities of all species in the capillary are known, the local conductivity κ can be computed:

$$\kappa(z,t) = F\left(m_H C_H(z,t) - \frac{m_{OH} K_w}{C_H(z,t)} + \sum_i C_i(z,t) \sum_j \alpha_{i,j}(z,t) Z_{i,j} m^0_{i,j}(z,t) \right) \tag{6}$$

where m_H and m_{OH} are the mobilities of hydrogen and hydroxyde ions respectively, F is Faraday's constant, C_H is the local concentration of hydrogen ions and K_w is the equilibrium constant of water.

The modified Ohm's law finally provides the means for calculating the local electric field strength E, knowing the electrical current density J, according to

$$E(z,t) = \frac{J}{\kappa(z,t)} \tag{7}$$

Eq. (7) is used for constant current densities. For constant voltage separations the total conductivity of the capillary determines the current density. This does not complicate calculations noticeably, yet it results in slightly more calculations being necessary.

When all component concentrations are known, the pH can be calculated by applying the charge balance equation

$$-\frac{\varepsilon}{F} \cdot \frac{\partial E(z,t)}{\partial z} = -C_H(z,t) + \frac{K_w}{C_H(z,t)} - \sum_i \sum_j Z_{i,j} \alpha_{i,j}(z,t) C_i(z,t) \tag{8}$$

where $Z_{i,j}$ is the charge of subspecies j of component i. It was shown [15] that the left-hand side of Eq. (8) (originating from the Maxwell's laws) can be of the order 10^{-7} mol/m^3 in isotachophoresis. It is expected to be significantly lower in zone electrophoresis making the assumption of electroneutrality a fair working approximation. All previous publications, except for Coxon et al. [16], assume electroneutrality in Eq. (8), which means that the left side is assumed to be zero.

Some authors have limited their model to strong ions [4], so that Eqs. (3)–(5) are not needed and Eq. (8) is simplified.

Of more practical value is the modelling of separations where weak ions are involved. Schwer et al. [6] solved Eq. (8) for cases where either H_3O^+ or OH^- were predominantly present, making the model somewhat simpler.

A refinement of the model that is sometimes used to enforce electro-neutrality, is the addition of a non-equal diffusion term [4,6]. This approach was not adopted here, because numerical experiments showed that it violated the mass-balance.

4. Numerical implementation

In order to solve Eq. (1) numerically it must first be written in a discrete version, which can be done in several ways, as will be shown later. After choosing appropriate space and time step values cyclic calculations on Eq. (1); Eq. (8) (using a central difference scheme for the electric field strength gradient); Eq. (3) and Eq. (4); Eq. (5); Eq. (6); Eq. (7) and finally Eq. (2) can sequentially be carried out.

4.1. Mesh widths

Unfortunately every numerical scheme comes with its own limitations concerning spatial (Δz) and temporal (Δt) mesh width size. If these limitations are disregarded, calculations will mostly result in fatal runaway situations. Numerical parameters involved in the process of choosing grid values are the cell Peclet number Pe and the Courant number Co.

$$Pe = \frac{v\Delta z}{D} \tag{9}$$

$$Co = \frac{v\Delta t}{\Delta z} \tag{10}$$

4.2. Test criteria

To be able to decide which numerical approach is best, one should define test criteria. Occurrence of oscillations and the magnitude of numerical diffusion are the main factors that determine the validity of the calculated result. First of all oscillations should be avoided, or minimized. If oscillations do occur at steep concentration gradients, one should not try correcting negative concentrations by setting them to zero, since this will definitely result in violation of the mass-balance [4]. Small overshoots are acceptable, provided that they do not lead to uncontrollable oscillations, violating the conservation of mass. Thus the most obvious test would be a mass-balance check, making sure that no material is produced or lost during calculations. The conservation of mass can simply be checked by calculating the total amount of each component at time t, and comparing it to the amount that was initially (before separation) present in the system.

For isotachophoretic (ITP) separations, the Kohlrausch regulating function [17] provides another means of checking the method's validity, when and where a steady-state is reached. Additionally, the computed boundary layer thickness of zones can be compared to theoretically predicted values. For strong electrolytes, Longsworth et al. [18] derived an analytical solution that was rearranged to [15]:

$$d = \frac{\ln(99)RT}{F\Delta E} \tag{11}$$

in which d is the distance over which a sample component concentration changes between 1 and 99% of its maximum value, R is the gas constant, T is the temperature and ΔE is the steady-state electric field strength difference on either side of the zone boundary.

4.3. The central difference scheme

The numerical scheme that is used most, is the central difference (CD) or forward time central space (FTCS) scheme [2,4,6].

$$C_z^{t+\Delta t} = C_z^t + \frac{D\Delta t}{(\Delta z)^2}\cdot(C_{z+\Delta z}^t - 2C_z^t + C_{z-\Delta z}^t) - \frac{\Delta t}{2\Delta z}\cdot(v_{z+\Delta z}^t C_{z+\Delta z}^t - v_{z-\Delta z}^t C_{z-\Delta z}^t) \tag{12}$$

This is a straightforward explicit scheme, that does not depend on the particular net migration direction of the component in control volume at z. The grid restrictions to avoid oscillations are that the absolute value of Pe should not be larger than 2 for any component, so that:

$$\Delta z \leq 2\frac{\min\limits_{i,z} D_i}{\max\limits_{i,z} |v_{i,z}|} \tag{13}$$

In addition, numerical stability of the explicit scheme requires that

$$\Delta t \leq \frac{1}{2}\frac{(\Delta z)^2}{\max\limits_i D_i} \text{ and } \Delta t \leq 2\frac{\min\limits_i D_i}{\max\limits_{i,z} v_{i,z}^2} \tag{14}$$

Simulation of transient capillary electrophoretic processes requires spatial resolution ranging from the (sub)micrometer level (during stacking) up to the (sub)millimeter level (during detection). For an efficient algorithm, this would require dynamic adaptation of Δz. In addition, in view of the quadratic interrelation between Δz and Δt in Eq. (14), this poses severe constraints on the computing time. For example with $\Delta z = 0.1$ μm, $\Delta t < 10$ μs is required. Simulation of stacking in a 1 mm plug for 1 s, not an unrealistic example, requires 10^9 calculation cycles. There is also no freedom to choose Δz and Δt independently. During stacking it may be necessary to choose a smaller Δz than the initial value. As pointed out by Dose [4], it is better to restart the simulation with a smaller Δz than to reduce Δz with all kinds of interpolations for concentrations, especially since this decrease in Δz will often only be necessary in the first few seconds of a simulation.

4.4. The upwind scheme

When choosing an upwind scheme, the direction of net migration in each individual element is taken into account. The absolute Pe value may exceed the formerly limiting value of 2, but the Co number is limited to a maximum value of 1.

If the local net migration velocity of a component is positive, the upwind discretization scheme is

$$C_z^{t+\Delta t} = C_z^t + \frac{D\Delta t}{(\Delta z)^2}\cdot(C_{z+\Delta z}^t - 2C_z^t + C_{z-\Delta z}^t) - \frac{\Delta t}{\Delta z}\cdot(v_z^t C_z^t - v_{z-\Delta z}^t C_{z-\Delta z}^t) \quad (15)$$

For oppositely directed convection, the convection term is adapted to incorporate elements that are located one grid step more in the positive direction of the z-axis.

There are two practical cases where the direction of overall migration of one and the same component can be different in different parts of the capillary: when the electroosmotic mobility and the electrophoretic mobility have opposite signs and in the case of ampholytes.

Until now both schemes (central difference and upwind) were used to calculate the concentration explicitly. An expectedly more stable scheme using implicit calculation of the concentration is the next step.

4.5. The implicit upwind scheme

The essential element of this approach is solving the equation implicitly for the concentration, and explicitly for the time-dependent velocities. Implicit calculation is inherently stable and poses no restrictions on Co values. This allows choosing Δz and Δt values independent from each other, resulting in a considerably faster algorithm.

The finite difference scheme of the model differential Eq. (1), for positive local net migration values at z, where C is taken implicitly and v explicitly, becomes:

$$C_z^{t+\Delta t} - \frac{D\Delta t}{(\Delta z)^2}\cdot(C_{z+\Delta z}^{t+\Delta t} - 2C_z^{t+\Delta t} + C_{z-\Delta z}^{t+\Delta t}) + \frac{\Delta t}{\Delta z}\cdot(v_z^t C_z^{t+\Delta t} + v_{z-\Delta z}^t C_{z-\Delta z}^{t+\Delta t}) = C_z^t \quad (16)$$

Since the velocity at time $t+\Delta t$ is not known, the old velocity is used here, which partially cancels the gained freedom in choice for Co.

In contrast to the scheme of Eq. (15), the implicit character of Eq. (16) forces it to be solved simultaneously for all z values. See Appendix 1 for an outline of the approach that was used to accomplish solving this and other implicit schemes.

4.6. An alternative scheme (DIME)

The implicit upwind scheme (Eq. (16)) couples velocities at time t to concentrations at time $t+\Delta t$. The larger the time step taken during calculation, the more the scheme will show inaccuracies. Therefore an intermediate scheme form taking the diffusion term implicitly, and the migration or convection term explicitly (DIME) was manufactured:

$$C_z^{t+\Delta t} - \frac{D\Delta t}{(\Delta z)^2}\cdot(C_{z+\Delta z}^{t+\Delta t} - 2C_z^{t+\Delta t} + C_{z-\Delta z}^{t+\Delta t}) = C_z^t - \frac{\Delta t}{\Delta z}\cdot(v_z^t C_z^t - v_{z-\Delta z}^t C_{z-\Delta z}^t) \quad (17)$$

4.7. Higher order schemes

To be able to cope with steep concentration gradients, better accuracy than provided by the above mentioned schemes —second order diffusion term, and a first order convection term— is needed. This can be achieved by applying higher order numerical schemes for the space discretization. Several different schemes can be implemented in one pass by introducing the curvature factor (CF) [19]. For implicit implementation of this concept, Eq. (16) needs to be rewritten as follows:

$$C_z^{t+\Delta t} - \frac{D\Delta t}{(\Delta z)^2}\cdot(C_{z+\Delta z}^{t+\Delta t} - 2C_z^{t+\Delta t} + C_{z-\Delta z}^{t+\Delta t}) + \frac{\Delta t}{\Delta z}\cdot(v_r^t C_r^{t+\Delta t} - v_\ell^t C_\ell^{t+\Delta t}) = C_z^t \quad (18)$$

where subscript ℓ refers to the left cell boundary and r to the right cell boundary. The velocity v_ℓ is the average value of the velocities in the control volumes at $z-\Delta z$ and z:

$$v_\ell^t = \frac{1}{2}(v_{z-\Delta z}^t + v_z^t) \quad (19)$$

For positive values of the left boundary velocity, C_ℓ is given by

$$C_\ell^{t+\Delta t} = \frac{1}{2}(C_{z-\Delta z}^{t+\Delta t} + C_z^{t+\Delta t}) - \beta_\ell(C_z^{t+\Delta t} - 2C_{z-\Delta z}^{t+\Delta t} + C_{z-2\Delta z}^{t+\Delta t}) \quad (20)$$

with β_ℓ being the CF, also determined by the velocity at the left cell boundary. Negative velocity values require adaptation of Eq. (20), and analogous expressions can be formulated for v_r and C_r. Depending on the chosen CF, a specific numerical scheme is selected (see Table 1). The QUICK (Quadratic Upstream Interpolation for Convective Kinematics) scheme being of the highest (third) order.

The above mentioned scheme can also be applied taking the migration term explicitly, as in the DIME scheme. In that case, Eq. (17) instead of Eq. (16) is rearranged in a manner analogous to Eqs. (18), (19), (20). The results of this effort will not be dealt with in the present paper.

Depending on the concentration gradient, different scheme orders can be applied to improve the accuracy of the results. In areas of low concentration gradients lower order schemes suffice and are preferred, because they do not introduce oscillations. More accurate higher order schemes are preferred in high concentration gradient areas, where lower order schemes would add significant numerical diffusion. A continuous transition from one scheme to another can be made using a variable curvature factor (VCF) also denoted by β in this paper.

Leonard et al. [20] presented the constraints that apply to VCF functions, and proposed several of these functions, using the normalized concentration $\tilde{C}_z$ in the control volume at z, defined by

$$\tilde{C}_z = \frac{C_z - C_{z-\Delta z}}{C_{z+\Delta z} - C_{z-\Delta z}} \quad \text{for } v_z > 0 \tag{21}$$

as running parameter. This makes implementing implicit calculation to its full extent merely impossible. Therefore all concentrations in Eq. (21) were taken at time t.

Leonard [19] proposed the EULER–QUICK function (Exponential Upwinding or Linear Extrapolation Refinement), given by:

for $\tilde{C}_z \le -1$ or $\tilde{C}_z \ge 1.5 \quad \beta = 0.125$

for $-1 < \tilde{C}_z \le 0 \quad \beta = \dfrac{0.5 + 0.125\tilde{C}_z}{1 - 2\tilde{C}_z}$

for $0.3 \le \tilde{C}_z \le 0.7$

$$\beta = 0.125 - 0.2609(\tilde{C}_z - 1.5) + 0.13613(\tilde{C}_z - 0.5)^2$$

for $0 < \tilde{C}_z < 0.3$ and $0.7 < \tilde{C}_z < 1$

$$\beta = \frac{\tilde{C}_z^2 - (1 + \tilde{C}_z)(\tilde{C}_z - 0.5) - \sqrt{\tilde{C}_z(1 - \tilde{C}_z)^3}}{(1 - 2\tilde{C}_z)^2}$$

for $1 \le \tilde{C}_z < 1.5 \quad \beta = \dfrac{\tilde{C}_z - 1}{2(2\tilde{C}_z - 1)}$

In addition to this the same author proposed the ULTRA–QUICK function (Universal Limiter for Tight Resolution and Accuracy) [20], reading:

for $\tilde{C}_z < 0 \quad \beta = 0.5$ (second order upwind)

for $0 \le \tilde{C}_z \le \dfrac{5}{6} \quad \beta = 0.125$ (QUICK)

for $\dfrac{5}{6} < \tilde{C}_z < 1 \quad \beta = \dfrac{\tilde{C}_z - 1}{2(1 - 2\tilde{C}_z)}$

for $\tilde{C}_Z \ge 1 \quad \beta = 0$ (second order central difference).

Both functions were implemented in the computer program and evaluated.

Table 1
Curvature factors (taken from Ref. [19])

Method	β	Order
QUICK	1/8	Third
	1/6	Second
Fromm	1/4	Second
2nd upwind	1/2	Second
Central difference	0	Second

5. Results and discussion

5.1. Computer program setup

In the MS-DOS based program the capillary was divided into three compartments of variable length, the composition of which could be chosen independently. Depending on the composition of the first and last compartment, either ITP or CZE mode of operation was possible. The inner diameter, driving current and calculation algorithm could be set in the

program editor, yet the latter two could also be changed during simulation. Capillary compositions could be saved in separate simulation files, so that simulations could be reloaded and continued later.

The simulation part of the program loaded a simulation file and if the simulation had not run before ($t=0$), the user could enter the physical length of the middle (injection) compartment, depending on the allowed range of Δz and Δt, which in turn depended on the algorithm chosen. During simulation, the value of Δt was automatically adjusted in such a way that a local *Co* value did not exceed a preset value. The physical length of the capillary could be infinitely long, which was achieved by calculating only in the range of the capillary where the sample concentration exceeded a predetermined threshold value, preferably corresponding to 1 molecule/volume element. Sample components were defined as components of which the initial concentration was non-zero in the middle compartment. If either side of this calculation range approached either end of the maximum number of grid points, the calculation range was shifted. If the calculation range tended to exceed the maximum number of grid points, Δz was doubled, adjacent elements were averaged and Δt was automatically adjusted.

Any of the following parameters could be plotted during simulation, and saved or loaded as a function of the position in the capillary: concentrations, linear velocities, *Pe* numbers, *Co* numbers, pH, electric field strength, conductivity, Kohlrausch regulating function value and charge excess. After choosing a detector location, time-based signals could also be displayed and saved.

The Windows based program differed mainly from the MS-DOS based version in the (virtually unlimited) available amount of memory, meaning that more space elements could be used, and the fact that the capillary could be divided into more than 3 compartments.

5.2. Simulations

The numerical implementation of several algorithms were tested and evaluated with different simulation conditions. The requirements were: absence of oscillations and numerical diffusion, correctly calculated steady state properties (concentrations, pH, field strengths) and satisfying mass balances. Numerical parameters were chosen such that realistic current densities (1–10 kA/m^2) could be simulated as well as realistic sample plug lengths (100–1000 μm). Local *Pe* numbers can thus easily be in the range 10–1000, quite impossible using a central difference approach. Time increments, Δt, however were automatically adjusted such that the maximum *Co* number remained smaller than a preset value.

5.3. Algorithm stability

Mosher et al. [2] mention that their numerical approach (central difference) was limited to low current densities in ITP, so that the relative contribution of diffusion was larger than in practice. The influence of the current density on numerical stability was investigated in a comparative study by Ermakov et al. [8], in which different numerical algorithms were applied to the isotachophoretic separation of 10 m*M* each of aniline and pyridine in 18 m*M* sodium–20 m*M* acetate as leading, and 40 m*M* β-alanine–50 m*M* acetate as terminator, at different currents in a 50 μm capillary. Of the finite difference schemes compared (the upwind Euler, central difference and artificial dispersion scheme) the latter was reported to perform best at both 0.05 and 0.2 μA. Higher currents were not possible due to substantial oscillations in the regions close to the zone boundaries. These results can be summarized in stating that the maximum local *Pe* number should not exceed 1.

In the implicit upwind scheme introduced in the present contribution, current densities up to 2.26 kA/m^2 (10 μA through a 75 μm I.D. capillary) can be simulated without oscillations. The previously mentioned numerical schemes were compared by simulating the steady-state of $44 \cdot 10^{-12}$ mol each of aniline and pyridine acetate in the above described electrolyte system, using a 75 μm I.D. capillary. Fig. 1a shows the results of the inherently stable implicit scheme. The mass balance was accurate within 1 ppm, and the boundary thickness was approximately 170 μm at a maximum *Pe* value of 26. Steady-state concentration levels were in accordance with Kohlrausch's law. When applying the hybrid DIME algorithm (Fig. 1b) the results are the same in all respects, except for the lesser degree of numerical

diffusion than the implicit scheme. This can be seen from the boundary layer thickness, which was approximately 120 μm.

Higher order schemes are specifically useful for the further decrease of numerical diffusion. For a CF value of zero (second order central difference) the boundary layer thickness is further decreased to 60 μm (Fig. 1c). This was only achieved at the cost of severe overshoot due to numerical dispersion at steep concentration boundaries, however these oscillations did not violate the mass balance.

A third order scheme, using a CF value of 1/8 (QUICK), resulted in boundary layer thickness values comparable to the second order central difference situation, yet showing less oscillations (Fig. 1d). The algorithms for Fig. 1c and d have less numerical diffusion when compared to the algorithms for Fig. 1a and b, as can be seen from the boundary layers. The oscillations seen in Fig. 1c and d indicate that numerical dispersion is becoming significant there. Increasing the CF value to 1/2 (second order upwind; Fig. 1e) did not result in dramatic improvements.

Variable curvature factor schemes applied to mulidimensional problems were reported to produce significantly more accurate solutions to diffusion convection problems, especially in the case of steep gradients [19,20]. Applying the suggested EULER–QUICK and ULTRA–QUICK schemes to the steady-state ITP situation led to unacceptable mass balance violation (Fig. 1f and g), which could possibly be caused by interference of the self correcting nature of ITP zone boundaries with this numerical approach. Additionally a slight deviation from Kohlrausch's law was observed.

5.4. Zone boundary thickness

A mixture of tetraalkylammonium ions were separated in ITP mode with 10 m*M* potassium acetate as

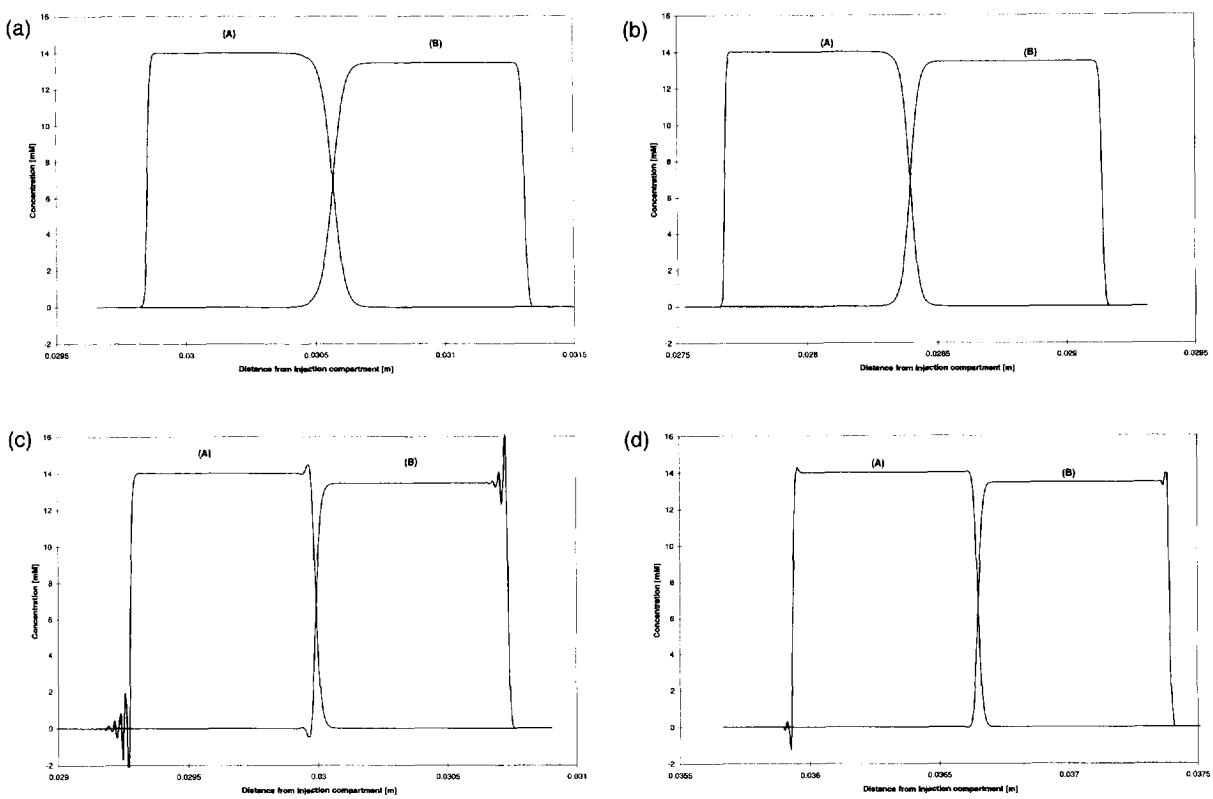

Fig. 1.

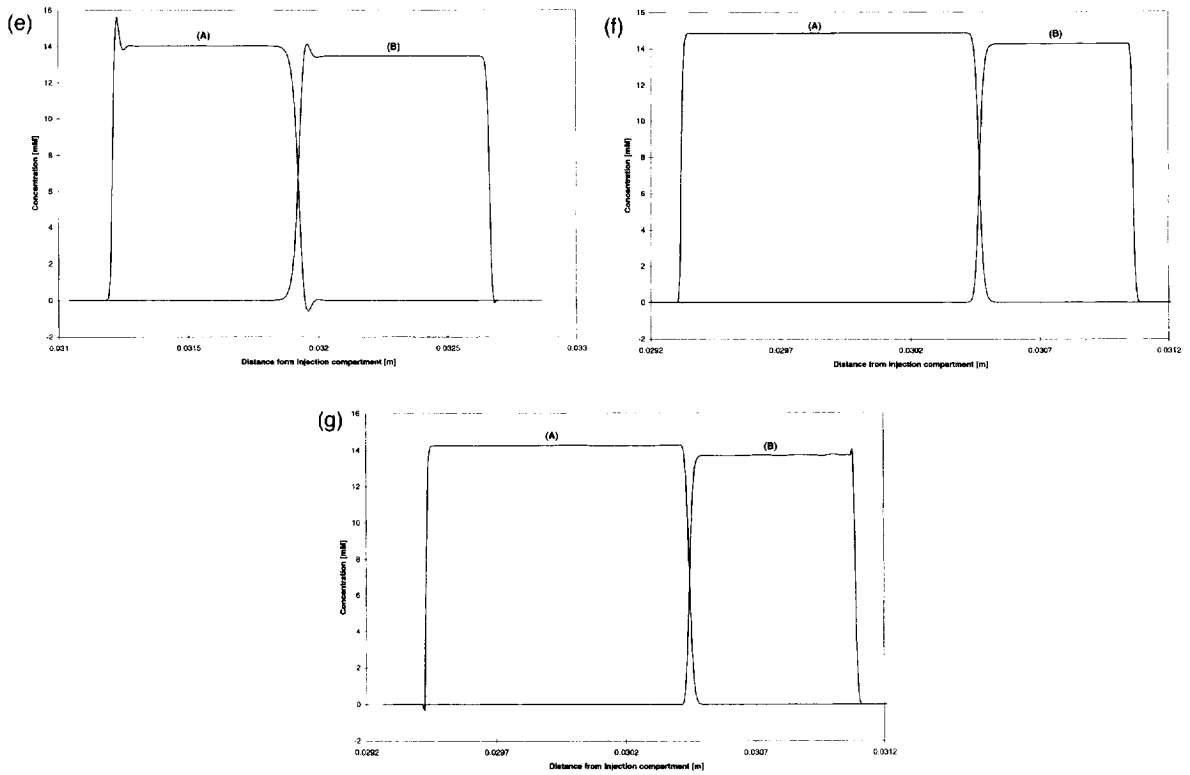

Fig. 1. Simulation of the isotachophoretic steady-state of the separation of 10 m*M* (A) aniline and (B) pyridine in a 18 m*M* sodium–20 m*M* acetate leading and 40 m*M* β-alanine–50 m*M* acetate terminator system. $Pe_{max}=26$. Algorithms: (a) Implicit upwind; (b) DIME (Diffusion Implicit Migration Explicit); (c) Second order central difference (CF=0); (d) QUICK (CF=1/8); (e) Second order upwind (CF=1/2); (f) EULER–QUICK; (g) ULTRA–QUICK.

leading (pH 4.75) and acetic acid as terminator, using the DIME scheme. From the resulting electric field strength results, graphically shown in Fig. 2, both ΔE and δ values were determined. The latter were also calculated from the former using Eq. (11). Table 2 summarizes the results, indicating that the zone boundary thickness is simulated in the right order of magnitude but that it is systematically higher than predicted. This was to be expected taking the relatively large mesh widths into account. The cause of this phenomenon is that, although the maximum *Co* number is restricted, local values can be much smaller (because of the uniform grid size), leading to damping. It is expected that better results will be achieved when using more grid points (smaller mesh widths).

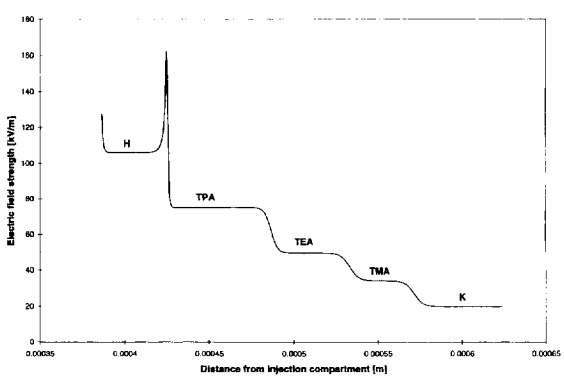

Fig. 2. Electric field strength distribution of the ITP steady-state of potassium (K, leading), tetramethyl (TMA), tetraethyl (TEA) and tetrapropylammonium (TPA) in 10 m*M* potassium acetate leading (pH 4.75) with acetic acid (H) as terminator. Algorithm: DIME ($Pe_{max}=46$).

Table 2
Estimation of the zone boundary thickness from simulation

Boundary	ΔE (kV/m)	d [Eq. (11)] (μm)	d (simulation) (μm)
Leading–1	8.7	14	10
1–2	15.7	8	10
2–3	20.8	6	10
3–terminator	43.4	3	8

5.5. Enforced configurations

Enforced configurations are sometimes encountered in isotachophoresis. These imply that the migration order in the steady-state does not coincide with the mobilities of the separands in their zone. Mosher et al. [2] gave the example of cycloserine in 10 m*M* sodium formate as a leading with formic acid (the H_3O^+ ion) as terminator. They calculated and measured (preparative setup) the properties of the steady-state zones. A comparison of these data to our simulation results, using the DIME scheme, can be found in Table 3. The simulations were carried out at 2.26 kA/m^2, so that the relative contribution of diffusion was more realistic than in Mosher's simulations. Naturally, steady-state composition does not depend on current density and the correlation of our results is striking. The pH and electric field strength distribution for the steady-state are shown in Fig. 3.

There is an enforced electric field strength step of the cycloserine zone that reaches out above the terminator level. The front of the sample zone is very sharp because of the large field strength gradient, but also because the effective mobility of cycloserine changes sign in the direction of the leading (pK_a values of the ampholyte are 4.4 and 7.4). The electric

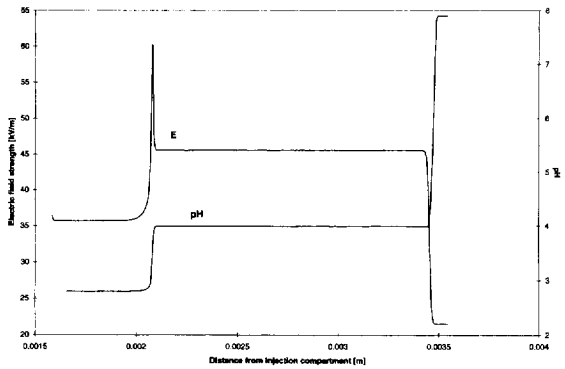

Fig. 3. Simulated local values of electric field strength and pH in an ITP steady-state of (left-to-right) formic acid (terminator), 0.44 pmol cycloserine (sample) and 10 m*M* sodium formate (leading) in a 75 μm capillary at 10 μA. Algorithm: DIME.

field strength overshoot at the rear of the sample zone is not an artifact: it was also observed experimentally. These kinds of physico-chemical overshoots can be mistaken for numerical artifacts, especially whilst they are being formed during simulation. On the other hand this phenomenon is well known amongst ITP analysts.

5.6. Application to CZE

In order to get an idea of how the presented approach would perform for CZE separations, the computer program was used to simulate peak splitting in case of severe sample overload as already investigated by Ermakov et al. [9,10]. It was shown that simulation of such phenomena can give valuable insight into their occurrence. A 2 mm injection plug of 20 m*M* pyridine was analysed in a BGE of 20 m*M*

Table 3
Calculated and experimentally determined composition of ITP steady-state

Zone	Leading			Cycloserine			Terminator		
	Lit	Exp	Mod	Lit	Exp	Mod	Lit	Exp	Mod
pH	7.88	5.90	7.9	3.95	4.00	3.99	2.77	2.82	2.79
Cond	108	80	110	52.6	43.7	49.7	71.5	60.0	63.4
Formic	10	–	10	8.78	–	8.7	18.1	–	18.0
Cycloserine	–	0	7.18	5.2	7.2	–	–	0	–

Lit: modelling results taken from [2]; Exp: experimental results taken from [2]; Mod: modelling results of the DIME algorithm.

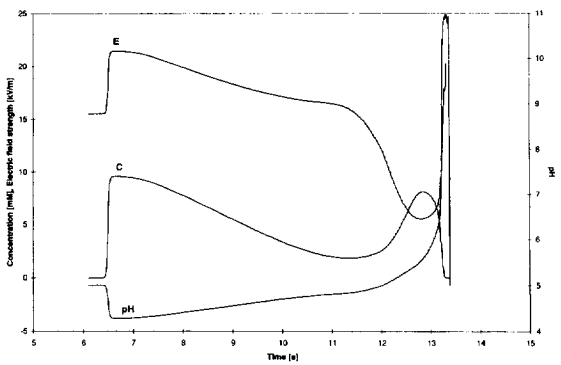

Fig. 4. Peak splitting of 20 m*M* pyridine in 20 m*M* acetate–sodium hydroxide at pH 4.5 in CZE mode. Algorithm: DIME.

acetate–sodium hydroxide (pH 4.5) at 2.26 kA/m^2. The electroosmotic mobility was set at $+40\cdot10^{-9}$ m^2/V s, corresponding to a ζ-potential of -50 mV. The detector was located at 10 mm from the start of the injection plug. The resulting pyridine concentration as a function of time is shown in Fig. 4.

As already pointed out by Ermakov, the pyridine is clearly split into 2 parts, the second of which moves with the electroosmotic velocity. In addition to the pyridine concentration, the local pH and fieldstrength are plotted as well. The latter explains especially why part of the pyridine remains in the injection plug: the local field strength in the sample zone is so low that the pyridine is trapped. In addition, the higher pH in the sample zone decreases the effective charge and velocity of pyridine. As explained in the original article, the occurrence of peak splitting depends on the sample concentration (below 5 m*M* it does not occur). It can be added that (at 20 m*M*) it also depends on the injection plug length: in a shorter plug, the field strength dip is smoothed out by diffusion sooner.

6. Conclusion

The developed computer program for the evaluation of several different numerical algorithms targeted at solving the electrophoretic convection–diffusion equation proved very useful. The user interface allowed switching easily from one algorithm to another. A way of practically implementing implicit computing of the differential equation is given.

Explicit central difference calculations, as used in several publications, were used as a starting point for developing faster and better algorithms, especially the restriction that the absolute *Pe* value should not exceed 2 caused this method to be rather unsuitable for simulating electrophoretic separations. This restriction was circumvented by rewriting the scheme into it's implicit form. Stable results not violating the mass-balance were obtained, be it that the boundary thicknesses did not conform to the Longsworth predicted values due to numerical diffusion. In this respect the proposed DIME scheme was the best first order scheme, whereas the purely third order QUICK scheme proved to be the best higher order scheme. Although fixed curvature factor methods like QUICK show little numerical diffusion, they also show small but stable concentration overshoots at sharp gradients for *Pe* values smaller than 10. For larger *Pe* values these methods become unstable. Of the order adaptive schemes, the EULER– QUICK method resulted in boundary thicknesses close to the predicted values, whereas the mass-balance was violated heavily for all *Pe* values. In contrast the ULTRA–QUICK method performed well, be it only at *Pe* values smaller than 10.

It turned out that all algorithms were to be used for specific limited situations only, depending on *Pe* and *Co* numbers. In general it was found that higher order algorithms generate better results than lower order algorithms, when looking at the zone boundary thickness.

Finally it should be stressed that being able to switch algorithms at any point during analysis is quite important, because during stacking an algorithm less sensitive to numerical oscillations is advisable. One could select an unconditionally stable lower order implicit algorithm during the stacking phase, followed by a higher order algorithm for sharpening up the steady state boundaries afterwards. The switching point depends on the maximum local *Pe* value in the simulated capillary.

7. List of symbols and abbreviations

Symbol	Description	Unit	Typical value/range	Occurrence
∂	Differential operator	–		Operator
α	Degree of dissociation	–	0.1	
δ	Defined as $\frac{D\Delta t}{(\Delta z)^2}$	–	Substitution	
ϵ	Dielectric constant	F/m	$7.08\cdot10^{-10}$	
κ	Conductivity	S/m		
τ	defined as $\frac{\Delta t}{\Delta z}$	s/m		Substitution
A	Matrix	–		
C	Concentration	mol/m^3	10^{-6}–10^{2}	
$\mathbf{C}$	Concentration vector	–		
Co	Courant number	–		
d	The distance over which a sample component concentration changes between 1 and 99% of its maximum value	m	10^{-5}	
D	Diffusion coefficient	m^2/s	10^{-10}–10^{-9}	
$\boldsymbol{D}$	Diffusion matrix	–		
eof	Electroosmotic flow	–		Subscript
E	Electric field strength	V/m	$\pm10^{5}$	
F	Faraday's constant	C/eq	96 485	Constant
H	Hydrogen			Subscript
i	Component number	–		Subscript
$\boldsymbol{I}$	Unity matrix	–		
j	Subspecies number	–		Subscript
J	Current density	A/m^2	$+/-10^{3}$	
K	Acid dissociation constant	–		
K_w	Dissociation constant of water at 298K	mol^2/m^6	10^{-8}	Constant
m	Effective mobility	$m^2/V\,s$	$+/-10^{-7}$	
m^0	Mobility at infinite dilution	$m^2/V\,s$	$+/-10^{-7}$	
m_H	Mobility of hydrogen ion	$m^2/V\,s$	$3.63\cdot10^{-7}$	Constant
m_{OH}	Mobility of hydroxide ion	$m^2/V\,s$	$-2.05\cdot10^{-7}$	Constant
$\boldsymbol{M}$	Migration matrix	–		
n	Number of charged subspecies	–		
N	Matrix dimension	–		
OH	Hydroxide	–		Subscript
p	Integer counter	–	1,2,...	
Pe	Peclet number	–		
q	Integer counter	–	1,2,...	
r	Integer counter		1,2,...	
$\mathbf{r}$	Boundary conditions vector	–		
R	Gas constant	J/mol K	8.3114	Constant
t	Time	s		Argument
v	Linear velocity	m/s	$+/-10^{-3}$	
w	Water	–		
z	Space coordinate, along the axis of the capillary	m		Argument
Z	Charge number	–		

Appendix 1

Matrix implementation of the convection–diffusion equation

For implicit calculations the set of convection–diffusion equations must be solved simultaneously for all z values. In order to do so, the equations are rewritten as an N by N matrix operation with the concentrations at t and $t+\Delta t$, $\mathbf{C}^t$ and $\mathbf{C}^{t+\Delta t}$ in vector notation, respectively, and the boundary conditions given in the vector r:

$$\boldsymbol{A}\cdot\mathbf{C}^{t+\Delta t}=\boldsymbol{C}^t+\mathrm{r} \qquad \text{(A–1)}$$

Matrix $\boldsymbol{A}$ can be defined as the sum of three matrices:

$$\boldsymbol{A}=(\boldsymbol{I}-\boldsymbol{D}+\boldsymbol{M}) \qquad \text{(A–2)}$$

where $\boldsymbol{I}$ is the unity matrix, $\boldsymbol{D}$ is a matrix solely containing diffusion term coefficients and $\boldsymbol{M}$ solely contains migration term coefficients. Numerical schemes that do not incorporate implicit calculation for either the diffusion term or the migration term in the original diffusion–convection equation, will have an all zero matrix $\boldsymbol{D}$ or $\boldsymbol{M}$, respectively. Eq. (A–1) can be solved with a simplified LU decomposition.

The lower, main and upper diagonal vectors in the tridiagonal matrix $\boldsymbol{A}$ are designated $A_{i,i-1}$, $A_{i,i}$ and $A_{i,i+1}$, respectively. Here i is used as a matrix element index. When defining δ and τ as

$$\delta=\frac{D\Delta t}{(\Delta z)^2} \qquad \text{(A–3)}$$

and

$$\tau=\frac{\Delta t}{\Delta z} \qquad \text{(A–4)}$$

the matrix elements, in the case of the implicit upwind scheme, for positive and negative net local migration velocities at z are given by

$$A_{i,i-1}=\delta-\tau\cdot v_{z-\Delta z} \quad \text{resp. } A_{i,i-1}=\delta \quad i=2(1)N$$

$$A_{i,i}=1-2\delta+\tau\cdot v_z$$

$$\text{resp. } A_{i,i}=1-2\delta-\tau\cdot v_z$$

$$i=1(1)N$$

$$A_{i,i+1}=\delta$$

$$\text{resp. } A_{i,i+1}=\delta+\tau\cdot v_{z+\Delta z} \quad i=1(1)N-1.$$

In view of the above, the boundary conditions r_z are only non-zero for the first ($z=1$) and last ($z=N$) control volume, again for positive and negative net local migration velocities at z respectively:

Table 4
Matrix and vector elements for different numerical schemes

		Matrix element					Vector element		
		$A_{i,i-2}$	$A_{i,i-1}$	$A_{i,i}$	$A_{i,i+1}$	$A_{i,i+2}$	C_i^t		
		$C_{z-2\Delta z}^{t+\Delta t}$	$C_{z-\Delta z}^{t+\Delta t}$	$C_z^{t+\Delta t}$	$C_{z+\Delta z}^{t+\Delta t}$	$C_{z+2\Delta z}^{t+\Delta t}$	$C_{z-\Delta z}^t$	C_z^t	$C_{z+\Delta z}^t$
Explicit central difference		0	0	1	0	0	$\delta+\frac{1}{2}\pi v_{z-\Delta z}^t$	$1-2\delta$	$\delta-\frac{1}{2}\pi v_{z+\Delta z}^t$
Explicit upwind	$v_z^t>0$	0	0	1	0	0	$\delta+\pi v_{z-\Delta z}^t$	$1-2\delta-\pi v_z^t$	δ
	$v_z^t<0$	0	0	1	0	0	δ	$1-2\delta+\pi v_z^t$	$\delta-\pi v_{z+\Delta z}^t$
Implicit upwind	$v_z^t>0$	0	$-\delta-\pi v_{z-\Delta z}^t$	$1+2\delta+\pi v_z^t$	$-\delta$	0	0	1	0
	$v_z^t<0$	0	$-\delta$	$1+2\delta-\pi v_z^t$	$-\delta+\pi v_{z+\Delta z}^t$	0	0	1	0
DIME	$v_z^t>0$	0	$-\delta$	$1+2\delta$	$-\delta$	0	$\pi v_{z-\Delta z}^t$	$1-\pi v_z^t$	0
	$v_z^t<0$	0	$-\delta$	$1+2\delta$	$-\delta$	0		$1+\pi v_z^t$	$-\pi v_{z+\Delta z}^t$
(V)CF	$v_\ell^t>0\wedge v_r^t>0$	$\beta_\ell\pi v_\ell^t$	$-\delta-(\frac{1}{2}+2\beta_\ell)\pi v_\ell^t-\beta_r\pi v_r^t$	$1+2\delta-(\frac{1}{2}-\beta_\ell)\pi v_\ell^t+(\frac{1}{2}+2\beta_r)\pi v_r^t$	$-\delta+(\frac{1}{2}-\beta_r)\pi v_r^t 0$		0	1	0
	$v_\ell t>0\wedge v_r^t<0$	$\beta_\ell\pi v_\ell^t$	$-\delta-(\frac{1}{2}+2\beta_\ell)\pi v_\ell^t$	$1+2\delta-(\frac{1}{2}-\beta_\ell)\pi v_\ell^t+(\frac{1}{2}+2\beta_r)\pi v_r^t$	$-\delta+\beta_\ell\pi v_\ell^t+(\frac{1}{2}-\beta_r)\pi v_r^t$	$-\beta_r\pi v_r^t$	0	1	0
	$v_\ell^t<0\wedge v_r^t>0$	0	$-\delta-(\frac{1}{2}-\beta_\ell)\pi v_\ell^t-\beta_r\pi v_r^t$	$1+2\delta-(\frac{1}{2}+2\beta_\ell)\pi v_\ell^t+(\frac{1}{2}+2\beta_r)\pi v_r^t$	$-\delta+\beta_\ell\pi v_\ell^t+(\frac{1}{2}-\beta_r)\pi v_r^t 0$		0	1	0
	$v_\ell^t<0\wedge v_r^t<0$	0	$-\delta-(\frac{1}{2}-\beta_\ell)\pi v_\ell^t$	$1+2\delta-(\frac{1}{2}+2\beta_\ell)\pi v_\ell^t+(\frac{1}{2}-\beta_r)\pi v_r^t$	$-\delta+\beta_\ell\pi v_\ell^t+(\frac{1}{2}+2\beta_r)\pi v_r^t$	$-\beta_r\pi v_r^t$	0	1	0

$r_1 = (-\delta + \tau \cdot v_0) \cdot C_0$ resp. $r_1 = -\delta \cdot C_0$

$r_N = -\delta \cdot C_{(N+1)\Delta z}$ resp.
$r_N = (-\delta - \tau \cdot v_{(N+1)\Delta z}) \cdot C_{(N+1)\Delta z}$

It is most convenient to take C_0^t and $C_{(N+1)\Delta z}^t$ as being equal to the invariant concentration in the left and right buffer vessel, respectively. For sample components these would normally be zero except during electrokinetic injection from one of the buffer vessels, as suggested by Dose [4]. By introducing invariance of the concentrations in the buffer vessels, it is not possible to describe buffer exhaustion in these compartments. When the buffer vessels in practice are large enough, noticeable exhaustion will not occur. Nevertheless, it could be interesting in some cases to study buffer exhaustion, imposing different boundary conditions, which is beyond the scope of this paper, especially since the one-dimensional case would not suffice to describe such phenomena.

With minor adaptations, an analogous strategy can be used for solving all other schemes mentioned in this paper. Table 4 lists the elements that make up $\boldsymbol{A}$ for those particular cases.

References

[1] F.M. Everaerts, J.L. Beckers, Th.P.E.M. Verheggen, Isotachophoresis — Theory, Instrumentation and Applications, (Journal of Chromatography Library, Vol. 6), Elsevier, Amsterdam, 1976.
[2] R.A. Mosher, D.A. Saville, W. Thormann, The Dynamics of Electrophoresis, VCH, Weinheim, 1992.
[3] H. Poppe, J. Chromatogr. 506 (1990) 45–60.
[4] E.V. Dose, G.A. Guiochon, Anal. Chem. 63 (1991) 1063–1072.
[5] S.V. Ermakov, O.S. Mazhorova, Yu.P. Popov, Informatica 3 (1992) 173–197.
[6] C. Schwer, B. Gas, F. Lottspeich, E. Kenndler, Anal. Chem. 65 (1993) 2108–2115.
[7] B. Gas, J. Chromatogr. 644 (1993) 161–174.
[8] S.V. Ermakov, M.S. Bello, P.-G. Righetti, J. Chromatogr. A 661 (1994) 265–278.
[9] S.V. Ermakov, M.Yu. Zhukov, L. Capelli, P.-G. Righetti, Anal. Chem. 66 (1994) 4034–4042.
[10] S.V. Ermakov, M.Yu. Zhukov, L. Capelli, P.-G. Righetti, Anal. Chem. 67 (1995) 2957–2965.
[11] J.C. Reijenga, E. Kenndler, J. Chromatogr. A 659 (1994) 403–417.
[12] T. Hirokawa, M. Nishimo, Y. Kiso, J. Chromatogr. 252 (1982) 49.
[13] T. Hirokawa, M. Nishimo, N. Aoki, Y. Kiso, Y. Sawamoto, T. Yagi, J.-I. Akiyama, J. Chromatogr. 271 (1983) D1–106.
[14] T. Hirokawa, Y. Kiso, B. Gas, I. Zuskova, J. Vacík, J. Chromatogr. 628 (1993) 283.
[15] J.C. Reijenga, Thesis, Eindhoven University of Technology, 1984.
[16] M. Coxon, M.J. Binder, J. Chromatogr. 95 (1974) 133–145.
[17] F. Kohlrausch, Ann. Phys. (Leipzig) 62 (1897) 209–216.
[18] D.A. MacInnes, L.G. Longsworth, Chem. Rev. 11 (1932) 171–230.
[19] B.P. Leonard, Int. J. Numer. Methods Fluids 8 (1988) 1291–1318.
[20] B.P. Leonard, S. Mokhtari, Int. J. Numer. Methods Eng. 30 (1990) 729–766.